Fabrication of CdSnP Thin Films by Phosphidation for Photovoltaic Application

AUTHOR(S):

Nakatsuka, Shigeru; Inoue, Ryosuke; Nose, Yoshitaro

CITATION:

Nakatsuka, Shigeru ...[et al]. Fabrication of CdSnP Thin Films by Phosphidation for Photovoltaic Application. ACS Applied Energy Materials 2018, 1(4): 1635-1640

ISSUE DATE:

2018-04-23

URL:

http://hdl.handle.net/2433/243851

Fabrication of $CdSnP_2$ Thin Films by Phosphidation for Photovoltaic Application

Shigeru Nakatsuka*, Ryosuke Inoue and Yoshitaro Nose

Department of Materials Science and Engineering, Kyoto University, Kyoto 606-8501, Japan

Keywords: II-IV-V_2, chalcopyrite, $CdSnP_2$, $ZnSnP_2$, phosphidation

* To whom all correspondence should be addressed. Tel.: +81-75-753-5472; Fax: +81-75-753-3579; E-mail: nakatsuka.shigeru.25c@kyoto-u.jp

Abstract

We report on the fabrication of $CdSnP_2$ thin films for photovoltaic application. The phosphidation method, where co-sputtered Cd-Sn precursor thin film reacts with phosphorus gas, was utilized for the preparation of $CdSnP_2$ thin films. In order to establish the fabrication process, the temperature dependence on product phases was investigated and $CdSnP_2$ thin films were obtained by the phosphidation at 350 °C for 30 min under the phosphorus vapor pressure of 10^{-2} atm. $CdSnP_2$ thin films showed a *n*-type conduction. The resistivity, the carrier concentration and the mobility were evaluated to be $3.5–3.7\times10^{2}$ Ω cm, $1–3\times10^{15}$ cm^{-3} and 4.7–17 cm^2 V^{-1} s^{-1}, respectively. $CdSnP_2$ thin films with relatively flat and smooth surface were obtained, although it was reported that $ZnSnP_2$ with the same crystal structure grew as the protrusion shape by the VLS growth mode. In order to investigate these difference in growth mechanism between $CdSnP_2$ and $ZnSnP_2$, the reaction process in Cd-Sn-P system was investigated and discussed based on the chemical potential diagrams. As the result, it was understood that Cd, Sn and P_4 directly reacted to form $CdSnP_2$, while $ZnSnP_2$ was formed via the reaction among Zn_3P_2, Sn and P_4 after Zn reacts with P_4 to produce Zn_3P_2. Therefore, it is speculated that simple reaction route results in the high growth speed and smooth flat morphology was obtained in the fabrication of $CdSnP_2$ thin films.

.

1. Introduction

$CuIn_{1-x}Ga_xSe_2$ (CIGS) and CdTe are promising materials for thin film photovoltaic devices. The solar cells based on these chalcogenide compounds recorded the high conversion efficiencies of 22.6 %[1] for CIGS and 22.1 %[2] for CdTe, respectively. However, the usage of rare or toxic elements prevents the widespread use of these compound semiconductors. From these backgrounds, materials composed of non-toxic and earth-abundant elements have been researched and $Cu_2ZnSnS_{4-x}Se_x$ achieved the high conversion efficiency of 12.6 %.[3] In addition, Cu_2SnS_3,[4] Cu_2O,[5] SnS,[6] FeS_2,[7] and Zn_3P_2[8] have been also investigated for the same concept.

$ZnSnP_2$ is also a promising material for solar absorber consisting of safe and earth-abundant elements. In the previous works, it was reported that $ZnSnP_2$ showed a *p*-type conduction with the carrier concentration of 10^{16}–10^{18} cm^{-3} and a direct bandgap of ~ 1.6 eV.[9–16] Based on Shockley-Queisser limit,[17] the theoretical conversion efficiency of about 30% is calculated in the single-junction solar cell using $ZnSnP_2$ under the condition of AM 1.5 G solar spectrum.[18] The absorption coefficient of $ZnSnP_2$ was reported to be approximately 10^5 cm^{-1} in visible light range,[18,19] which is comparable to that of CIGS.[18,20] Our research group reported that solar cells using $ZnSnP_2$ thin films[21] and bulk crystals [15,22,23]. The solar cells using $ZnSnP_2$ bulk crystals recorded the best conversion

efficiency of 3.44 % (J_{SC} = 12.3 mA/cm^2, V_{OC} = 0.472 V, FF = 0.594).[23] The solar cell structure was Al/ZnO;Al/ZnO/(Cd,Zn)S/$ZnSnP_2$/Cu. In this device, the value of V_{OC} was largely low considering the bandgap of $ZnSnP_2$. XPS measurements revealed that CdS/$ZnSnP_2$ showed a large conduction band offset, ΔE_C = –1.2 eV,[24] which suggested that band alignment was– necessary to achieve a high conversion efficiency.

In this study, we focused on $CdSnP_2$ as a *n*-type material in the $ZnSnP_2$ solar cells. $CdSnP_2$ has a chalcopyrite structure as well as $ZnSnP_2$ and its bandgap is 1.17 eV.[25] Kumagai *et al*. carried out the first-principles calculation in $ZnSnP_2$ with chalcopyrite structure to obtain its band structure.[26] They reported that the valence band maximum (VBM) at the Γ point is mainly composed of P orbitals with slight hybridization with Zn and Sn orbitals and the conduction band minimum (CBM) is primarily composed of Zn and Sn cations orbitals. Consequently, the level of VBM in $CdSnP_2$ might be similar to that in $ZnSnP_2$ because of the same crystal structure and anions. This results in the ΔE_C value of − 0.5 eV between $ZnSnP_2$ and $CdSnP_2$ considering the difference of bandgap in both compounds and the improvement of band alignment is expected compared to CdS. In addition, it was reported that $ZnSnP_2$ and $CdSnP_2$ form a solid solution in all composition range,[27] which suggests the intermixing of Zn and Cd atoms at $CdSnP_2$/$ZnSnP_2$ interface and *pn*-junction with few band offset and interfacial defect can

be formed. However, few reports on the formation of $CdSnP_2$ thin films are available.

In this report, we thus tried to establish the fabrication process to obtain $CdSnP_2$ thin films, where Cd-Sn precursor thin films react with phosphorus gas, so-called phosphidation. Particularly, the impact of reaction temperature on product phases was investigated and morphology change was discussed based on the chemical potential diagrams.

2. Experimental method

Cd-Sn thin films with the thickness of 0.5 μm were fabricated as a precursor on soda lime glass substrates by magnetron direct current sputtering with a base pressure of 5×10^{-4}Pa. The 1 inch target materials of Cd (99.9 %, Kojundo Chemical Laboratory) and Sn (99.99%, Furuuchi Chemical) were co-sputtered for 45 min under an Ar atmosphere with the pressure of 0.8 Pa and the gas flow rate of 20 sccm. The power densities for Cd and Sn targets were set at 0.6 and 3.2 W/cm^2, respectively. During the sputtering, the substrates were rotated at 12 rpm without heating. For the safety sputtering of Cd, the target materials were sufficiently cooled down for more than 30 min. Dust collecting should be utilized when sample are extracted from a sputtering chamber. The thickness and composition were measured by inductively coupled plasma-atomic emission spectroscopy (ICP-AES, SII Nano Technology SPS3520UV). The samples were

dissolved in inverse aqua regia (HNO_3:HCl = 3:1) and the solution 1/10-diluted with deionized water was used for the ICP-AES measurements. Considering the higher vapor pressure of Cd, the molar ratio [Cd]/[Sn] was controlled to be about 1.2 in the precursor thin films.

Then, Cd-Sn thin films reacted with phosphorus gas to obtain $CdSnP_2$ thin films by phosphidation. The details of the experimental conditions were described in our previous work.[28] We used two phase sample with Sn and Sn_4P_3 as a phosphorus source and phosphorus gas was transported to the precursor thin films using Ar carrier gas, which was deoxidized by passing through a Ti sponge heated at 900 °C. The partial pressure of phosphorus was set at approximately 10^{-2} atm by controlling the temperature of two phase sample. In this study, the phosphidation temperatures were 300, 350 and 400 °C. After the phosphidation, the thin films were cooled down in the furnace by turning off the heater, or quenched outside the furnace. The surficial and cross-sectional morphology of thin films before and after phosphidation were analysed by scanning electron microscopy (SEM, HITACHI S-3500H and HITACHI SU-1500) The product phases were identified by X-ray diffraction (XRD, Panalytical X'Pert Pro Alpha-1), where CuKα1 (λ=1.5406 Å) was used as an incident X-ray (45 kV,40 mA) in Bragg–Brentano (θ–2θ) configuration.

In order to evaluate the electrical properties, Hall effect and resistivity measurements

were carried out at room temperature based on van der Pauw method using Hall-resistivity measurement system (Toyo Technica, ResiTest8300).

For the consideration of growth mechanism in the phosphidation method, we used the chemical potential diagrams. The review on the chemical potential diagrams is well summarized by Yokokawa.[29] A chemical potential diagram shows a stable potential region in various substances and each axis represents a chemical potentials of constituent elements. The chemical potential diagram of the Cd-Sn-P system was drawn using the software, Chesta 3.2.6.9, developed by Hatada. In order to obtain the potential diagrams, the thermodynamic data for Cd (g) and Sn (g) were derived from the database edited by Barin[30]. The Gibbs energies of formation for CdP_2 (s), Cd_3P_2 (s) and $CdSnP_2$ (s) reported by Sirota *et al.*[31] and Smolyarenko *et al.*[32] were also utilized.

3. Results and discussion

3.1. Effect of phosphidation temperature

In order to obtain $CdSnP_2$ thin films with the single-phase, the phosphidation of Cd-Sn precursor thin films was carried out at various reaction temperatures such as 300, 350 and 400 °C. In each experiment, Cd-Sn precursor thin films reacted with phosphorus gas for 30 min and then was cooled down in the furnace. Figure 1 shows the XRD profiles of Cd-Sn precursor thin films before and after phosphidation. In the precursor thin film, Cd and

Sn were identified and alloy was not observed, because Cd-Sn system is a typical eutectic system. The formation of $CdSnP_2$ as a main phase was observed in the phosphidation at 300 and 350 °C. In particular, all reflections observed in the sample prepared at 350 °C were corresponded to the reflections of $CdSnP_2$. In addition, those samples show (112) plane orientation of $CdSnP_2$, which is a close-packed plane in chalcopyrite structure. ICP-AES analysis showed that the composition of the thin film fabricated at 350 °C was 27.2 at. % Cd, 23.6 at. % Sn and 53.2 at.% P, which is Cd-rich composition compared with the stoichiometric ratio of $CdSnP_2$. In some samples prepared by the same condition, Cd_3P_2 was identified from XRD profiles. Therefore, the existence of Cd_3P_2 as a secondary phase is considered even in the case that Cd_3P_2 is not identified in XRD profiles as shown in Fig. 1. While, Cd_6P_7 and Sn were identified in addition to $CdSnP_2$ in the sample for 400 °C.

Figure 2 shows SEM images of Cd-Sn precursor thin films before and after phosphidation. The Cd-Sn precursor thin film was composed of sub-micron particles. On the other hand, the sub-micron particles were not observed in the thin film after phosphidation at 300 °C, which was the morphology indicating that metal precursor melted. The phosphidation at 350 °C resulted in the $CdSnP_2$ thin film consisting of particles with the diameter of about 1 μm. The particles with the diameter of a few μm

were formed on the surface of the thin film in the sample after phosphidation at 400 °C. Such particles might be secondary phases containing Sn. The cross-sectional SEM observation was carried out in Cd-Sn precursor thin film and $CdSnP_2$ thin film fabricated by the phosphidation at 350 °C as shown in Fig. 3. In the Cd-Sn precursor thin film, it is observed that sub-micron particles were deposited on the glass substrate, while $CdSnP_2$ film shows the dense microstructure consisting of granular particles compared with the Cd-Sn precursor thin film. This implies that phosphidation reaction proceeded as metal precursor partly-melted. In addition, it is confirmed that the thickness of the film was reduced, which might be attributed to the evaporation of precursor metal. ICP-AES analysis also clarified that a half amount of precursor metal, Cd and Sn, evaporated during the phosphidation experiments at 350 °C, which has to be improved in future work. The Hall measurement indicates that $CdSnP_2$ thin films prepared by the phosphidation has the *n*-type conduction as well as the $CdSnP_2$ bulk crystals grown by the solution method.[25] $CdSnP_2$ thin films showed a *n*-type conduction. The resistivity, the carrier concentration and the mobility were evaluated to be $3.5–3.7\times10^2$ Ω cm, $1–3\times10^{15}$ cm^{-3} and 4.7–17 cm^2 V^{-1} s^{-1}, respectively.

As mentioned above, $CdSnP_2$ thin films were obtained by the phosphidation of Cd-Sn precursor thin films at 350 °C for 30 min. In addition, $CdSnP_2$ thin films has relatively

smooth morphology compared with $ZnSnP_2$ thin films. In our previous work, a different surface morphology was observed in $ZnSnP_2$ thin films fabricated even by a similar phosphidation process.[28] Some $ZnSnP_2$ protrusions with the length of a few μm were formed on the $ZnSnP_2$ thin film by so-called VLS (Vapor-Liquid-Solid) growth mode.[28,33] It is interesting that $CdSnP_2$ and $ZnSnP_2$ showed different morphologies in spite of the similarity in constituent elements and crystal structures.

3.2. Growth mechanism of $CdSnP_2$ thin film

The time dependence of phosphidation in $CdSnP_2$ was investigated in order to clarify the growth mechanism. Here, we prepared a sample discontinued at 250 °C on the way heating up to 300 °C and another one after the phosphidation of Cd-Sn thin film at 300 °C for 2 min. Each sample was quenched outside the furnace in order to freeze the state during the phosphidation, while samples as shown in the previous section were conventionally cooled in the furnace after phosphidation. Figure 4 shows the XRD profile for each sample. The discontinued sample indicates that phosphidation reaction had not started at the heating stage because precursor metals such as Cd and Sn were identified. On the other hand, $CdSnP_2$ is observed as a main phase even in the phosphidation for 2 min, which suggests that the reaction rate to form $CdSnP_2$ is higher compared with $ZnSnP_2$ fabricated by the same phosphidation method. In the case of $ZnSnP_2$, 5 min

phosphidation did not finish the formation of $ZnSnP_2$ even in the higher reaction temperature of 450 °C. It is also understood that partly-melted precursor metal is an important factor for fast phosphidation reaction from the SEM images of the film surface shown in Figure 5, as previously predicted.

Here, the difference of the surface morphologies between $CdSnP_2$ and $ZnSnP_2$ films is discussed. In this study, we consider the difference in growth mechanism between both based on the chemical potential diagrams, because the morphology might depend on the growth mechanism of each thin film. Figure 6 shows the chemical potential diagrams of the Cd-Sn-P system at 300 °C together with the diagram of the Zn-Sn-P system at 450 °C, which was previously reported by our group. [28] The logarithms of the partial pressures of Cd (g), Zn (g), Sn (g) and P_4 (g) were used as the axes, which represent their chemical potentials. The dotted line indicates the partial pressure of P_4 (g) controlled in the experiments: 10^{-2} atm.

We discuss the phosphidation process of Cd-Sn precursor thin films as well as the case of Zn-Sn films. The point A in Figure 6a represents the state for Cd-Sn precursor thin films before phosphidation. Then, the chemical potential of phosphorus in the film increases with keeping the equilibrium of Cd (l) and Sn (l) as the phosphidation reaction proceeds, and at the point B, $CdSnP_2$ (s) forms. On the other hand, in the Zn-Sn-P system

shown in Figure 6b, the phosphorus potential for the formation of $ZnSnP_2$ (s) shown by point D is much higher than that for Zn_3P_2 (s) shown by point C. It is thus understood that the formation of Zn_3P_2 (s) preferentially occurs before $ZnSnP_2$ (s) in the Zn-Sn-P system. Such a behaviour was experimentally observed in our previous work.[28] The previous work also showed that the surface morphology of $ZnSnP_2$ thin films was rough and some protrusions were grown. To discuss the roughness of $ZnSnP_2$ thin films, two issues during phosphidation should be considered. One is the microstructure of the Zn-Sn precursor thin films before phosphidation, where it was observed that the separation of Zn and Sn grains and the cohesion of Sn with the grain size of a few micron. The separation is expected from the phase diagram of the Zn-Sn system. The other one is a phosphidation process, which was investigated experimentally and thermodynamically. The formation of $ZnSnP_2$ protrusions by VLS growth mode is due to the above two issues. On the other hand, the grain size in Cd-Sn precursor thin films is sub-micron as shown in Figure 2a although the separation of Cd and Sn is observed. In addition, the equilibrium chemical potential of phosphorus with $CdSnP_2$ is lower than that with Cd_3P_2 as shown in Figure 6a, which suggests that $CdSnP_2$ forms without the formation of other phases as described above. These are different with the case of $ZnSnP_2$, and key conditions to obtain a smooth surface of $CdSnP_2$ films.

4. Conclusions

In this study, we investigated the temperature dependence in phosphidation of Cd-Sn thin films on product phases and $CdSnP_2$ thin films were prepared at 350 °C for 30 min under the phosphorus vapor pressure of 10^{-2} atm. $CdSnP_2$ thin films showed a *n*-type conduction. $CdSnP_2$ thin films showed a *n*-type conduction. The resistivity, the carrier concentration and the mobility were evaluated to be $3.5–3.7\times10^{2}$ Ω cm, $1–3\times10^{15}$ cm^{-3} and 4.7–17 cm^{2} V^{-1} s^{-1}, respectively. The SEM observation suggested that $CdSnP_2$ thin films with relatively flat and smooth surface were obtained, although the formation of $ZnSnP_2$ protrusions by the VLS growth mode was reported in the case of the Zn-Sn-P system. In order to investigate the difference in both systems, the reaction process in the Cd-Sn-P system was investigated and discussed based on the chemical potential diagrams. The experimental results and the chemical potential diagram suggested that Cd, Sn and P_4 directly reacted to form $CdSnP_2$, while $ZnSnP_2$ was formed via the reaction among Zn_3P_2, Sn and P_4 after Zn reacts with P_4 to produce Zn_3P_2. Therefore, it is concluded that direct reaction route to form $CdSnP_2$ results in the high growth rate and flat morphology in the fabrication of $CdSnP_2$ thin films.

Acknowledgements

The authors wish to thank Assistant Prof. N. Hatada (Kyoto Univ.) for the provision of Chesta, software for creating chemical potential diagrams. This work was financially supported by JST CREST Grant Number JPMJCR17J2, The Mitsubishi Foundation and Grant-in-Aid for JSPS Research Fellow Number 16J09443.

References

(1) Jackson, P.; Wuerz, R.; Hariskos, D.; Lotter, E.; Witte, W.; Powalla, M. Effects of Heavy Alkali Elements in Cu(In,Ga)Se_2 Solar Cells with Efficiencies up to 22.6%. *Phys. Status Solidi RRL* **2016**, *10*, 583‑586.

(2) First Solar. Fist Solar Hits Record 22.1% Conversion Efficiency for CdTe Solar Cell. https://www.greentechmedia.com/articles/read/First-Solar-Hits-Record-22.1-Conversion-Efficiency-For-CdTe-Solar-Cell (last accessed January 2018).

(3) Wang, W.; Winkler, M. T.; Gunawan, O.; Gokmen, T.; Todorov, T. K.; Zhu, Y.; Mitzi, D. B. Device Characteristics of CZTSSe Thin-Film Solar Cells with 12.6% Efficiency. *Adv. Energy Mater.* **2014**, *4*, 1301465.

(4) Nakashima, M.; Fujimoto, J.; Yamaguchi, T.; Izaki, M. Cu_2SnS_3 Thin-Film Solar Cells Fabricated by Sulfurization from NaF/Cu/Sn Stacked Precursor. *Appl. Phys. Express* **2015**, *8*, 42303.

(5) Minami, T.; Nishi, Y.; Miyata, T. Heterojunction Solar Cell with 6% Efficiency Based on an N-Type Aluminum-Galium-Oxide Thin Film and P-Type Sodium-Doped Cu_2O Sheet. *Appl. Phys. Express* **2015**, *8*, 22301.

(6) Sinsermsuksakul, P.; Sun, L.; Lee, S. W.; Park, H. H.; Kim, S. B.; Yang, C.; Gordon, R. G. Overcoming Efficiency Limitations of Sn-S-Based Solar Cells. *Adv.*

Energy Mater. ***2014***, *4 , 1400496.*

(7) Ennaoui, A.; Tributsch, H. Iron Sulphide Solar Cell. *Sol. Cells* **1984**, *13*, 197‐200.

(8) Bhushan, M.; Catalano, A. Polycrystalline Zn3P2 Schottky Barrier Solar Cells. *ppl. Phys. Lett.* **1981**, *38*, 39‐41.

(9) Abdurakhimov, A. A.; Kradinova, L. V.; Parimbekov, Z. A.; Rud’, Y. V. chottky Diodes Made of P-Type ZnSnP2. *Sov. Phys. Semicond.* **1982**, *16*, 156‐59.

(10) Ryan, M. A.; Peterson, M. W.; Williamson, D. L.; Frey, J. S.; Maciel, G. E.; arkinson, B. A. Metal Site Disorder in Zinc Tin Phosphide. *J. Mater. Res.* **1987**, , 528‐537.

(11) Nakatsuka, S.; Nakamoto, H.; Nose, Y.; Uda, T.; Shirai, Y. Bulk Crystal Growth nd Characterization of $ZnSnP_2$ Compound Semiconductor by Flux Method. *Phys. Status Solidi C* **2015**, *12*, 520‐523.

(12) Scanlon, D. O.; Walsh, A. Bandgap Engineering of $ZnSnP_2$ for High-Efficiency Solar Cells. *Appl. Phys. Lett.* **2012**, *100*, 251911.

(13) Hinuma, Y.; Oba, F.; Nose, Y.; Tanaka, I. First-Principles Study of Valence Band Offset at $ZnSnP_2$/CdS, $ZnSnP_2$/ZnS, and Related Chalcopyrite/Zincblende Heterointerfaces. *J. Appl. Phys.* **2013**, *114*, 043718.

(14) Ajmera, P. K.; Shin, H. Y.; Zamanian, B. Vacuum Growth of Thin Films of $ZnSnP_2$.

Sol. Cells **1987**, *21*, 291–299.

(15) Nakatsuka, S.; Yuzawa, N.; Chantana, J.; Minemoto, T.; Nose, Y. Solar Cells Using Bulk Crystals of Rare Metal-Free Compound Semiconductor $ZnSnP_2$. *Phys. Status Solidi A* **2017**, *214*, 1600650.

(16) Nakatani, K.; Minemura, T.; Miyauchi, K.; Fukabori, K.; Nakanishi, H.; Sugiyama, M.; Shirakata, S. Photoluminescence Property of $ZnSnP_2$ by Solution Growth and Normal Freezing Methods. *Jpn. J. Appl. Phys.* **2008**, *47*, 5342–5344.

(17) Shockley, W.; Queisser, H. J. Detailed Balance Limit of Efficiency of PN Junction Solar Cells. *J. Appl. Phys.* **1961**, *32*, 510–519.

(18) Yokoyama, T.; Oba, F.; Seko, A.; Hayashi, H.; Nose, Y.; Tanaka, I. Theoretical Photovoltaic Conversion Efficiencies of $ZnSnP_2$, $CdSnP_2$, and $Zn_{1-x}Cd_xSnP_2$ Alloys. *Appl. Phys. Express* **2013**, *6*, 61201.

(19) Shin, H. Y.; Ajmera, P. K. Characterization of Vacuum Grown Thin Films of $ZnSnP_2$. *Mater. Lett.* **1987**, *5*, 211–214.

(20) Minoura, S.; Kodera, K.; Maekawa, T.; Miyazaki, K.; Niki, S.; Fujiwara, H. Dielectric function of Cu(In,Ga)Se_2-Based Polycrystalline Materials. *J. Appl. Phys.* **2013**, *113*, 63505.

(21) Yuzawa, N.; Chantana, J.; Nakatsuka, S.; Nose, Y.; Minemoto, T. $ZnSnP_2$ thin-

film solar cell prepared by phosphidation method under optimized Zn/Sn atomic ratio of its absorbing layer. *Curr. Appl. Phys.* **2017**, *17* , 557–564.

(22) Nakatsuka, S.; Akari, S.; Chantana, J.; Minemoto, T.; Nose, Y. Impact of Heterointerfaces in Solar Cells Using $ZnSnP_2$ Bulk Crystals. *ACS Appl. Mater. Interfaces* **2017**, *9*, 33827–33832.

(23) Akari, S.; Chantana, J.; Nakatsuka, S.; Nose, Y.; Minemoto, T. $ZnSnP_2$ Solar Cell with (Cd,Zn)S Buffer Layer: Analysis of Recombination Rates. *Sol. Energy Mater. Sol. Cells* **2018**, *174*, 412–417.

(24) Nakatsuka, S.; Nose, Y.; Shirai, Y. Band Offset at the Heterojunction Interfaces of CdS/$ZnSnP_2$, ZnS/$ZnSnP_2$, and In_2S_3/$ZnSnP_2$. *J. Appl. Phys.* **2016**, *119*, 193107.

(25) Shay, J. L.; Wernick, J. H. *Chalcopyrite Semiconductors: Growth, Electronic Properties, and Applications*; Pergamon Press: Oxford, 1975.

(26) Kumagai, Y.; Choi, M.; Nose, Y.; Oba, F. *Phys. Rev. B* First-principles study of point defects in chalcopyrite ZnSnP2. *Condens. Matter Mater. Phys.* **2014**, *90*, 1‑12.

(27) Higashino, T.; Nose, Y.; Toyoura, K.; Uda, T. *Bulk Crystal Growth of Chalcopyrite Semiconductors of the Zn-Cd-Sn-P System Based on the Phase Diagram*. MRS Fall Meeting, Boston, USA, Nov 28−Dec 2, 2011.

(28) Nakatsuka, S.; Nose, Y.; Uda, T. Fabrication of ZnSnP2 thin films by phosphidation. *Thin Solid Films* **2015**, *589*, 66‐71.

(29) Yokokawa, H. Generalized Chemical Potential Diagram and Its Applications to Chemical Reactions at Interfaces Between Dissimilar Materials. *J. Phase Equilibria* **1999**, *20*, 258‐287.

(30) Barin, I. *Thermochemical Data of Pure Substances, third ed.*; VCH Verlagsgesellschaft GmbH: Weinheim, 1995.

(31) Sirota, N. N., Antyukhov, A. M., Smolyarenko, E. M. Investigation into Thermodynamic Properties of Cd-P System Compound by Electromotive Forces Method. *Dokl. Akad. Nauk SSSR* **1974**, *219*, 397.

(32) Smolyarenko, E. M. Yakimovich, V. N. Thermodyanamics of Formation of $ZnSnP_2$ and $CdSnP_2$. *Izv. Akad. Nauk SSSR, Neorg. Mater* **1981**, *17*, 132‐134.

(33) Wagner, R. S.; Ellis, W. C. Vapor-Liquid-Solid Mechanism of Single Crystal Growth. *Appl. Phys. Lett.* **1964**, *4*, 89–90.

■ Figure captions

Figure 1. XRD profiles of Cd-Sn thin films before and after phosphidation for 30 min at various temperaturese.

Figure 2. SEM images of Cd-Sn thin films before and after phosphidation for 30 min at various temperatures.

Figure 3. Cross-sectional SEM images of Cd-Sn thin films (a) before and (b) after phosphidation at 350 °C.

Figure 4. XRD profiles of Cd-Sn thin films before and after phosphidation at 300 °C. “Discontinued” indicates the sample discontinued on the way heating up to 300 °C.

Figure 5. SEM images of thin films (a) before phosphidation, (b) discontinued during heating up, and after phosphidation at 300 °C (c) 5 min and (d) 30 min.

Figure 6. Chemical potential diagrams of (a) Cd-Sn-P system at 300 °C and (b) Zn-Sn-P system at 450 °C.

■ Figures

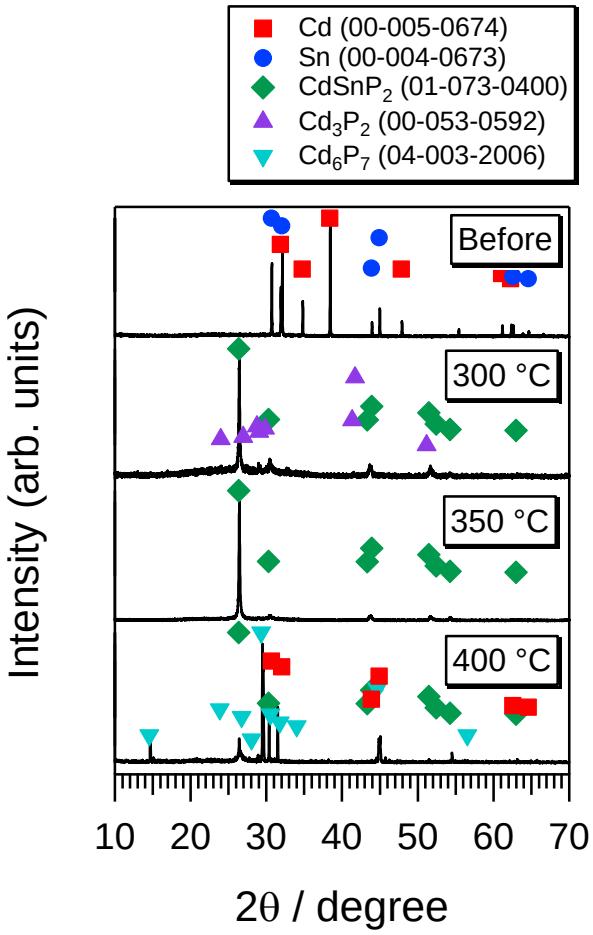

Fig. 1. XRD profiles of Cd-Sn thin films before and after phosphidation for 30 min at various temperaturese.

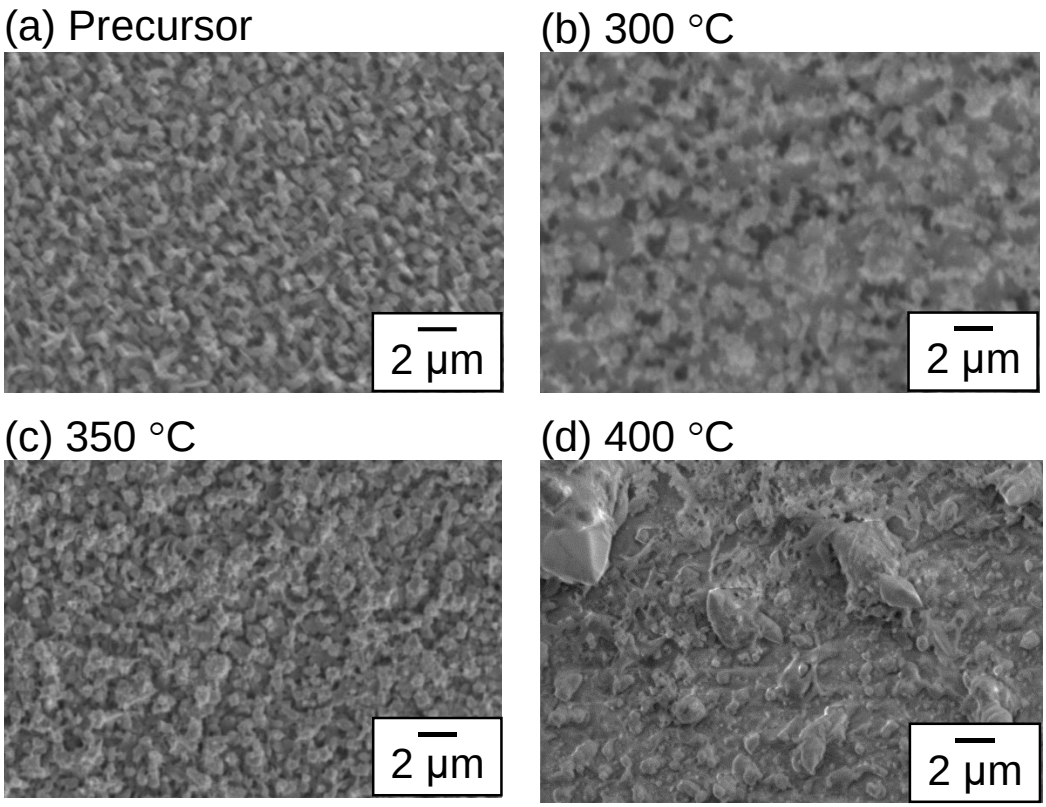

Fig. 2. SEM images of Cd-Sn thin films before and after phosphidation for 30 min at various temperatures.

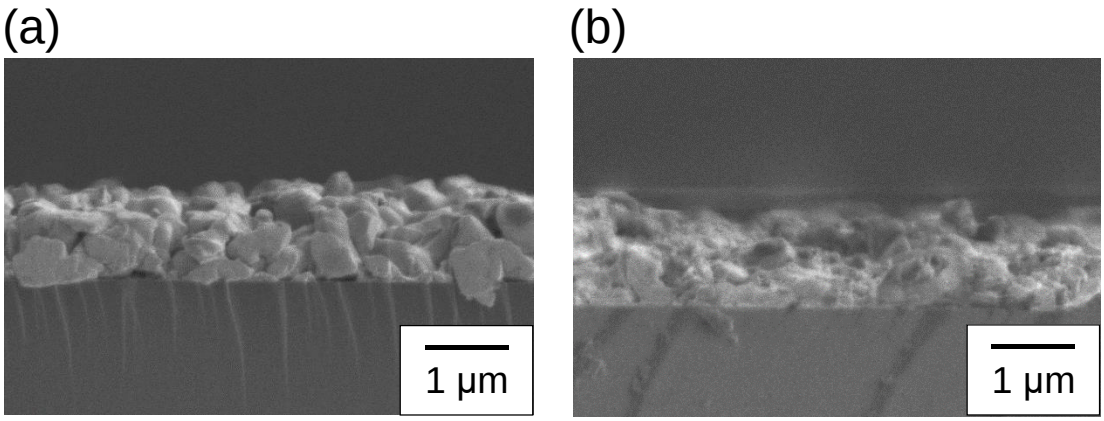

Fig. 3. Cross-sectional SEM images of Cd-Sn thin films (a) before and (b) after phosphidation at 350 °C.

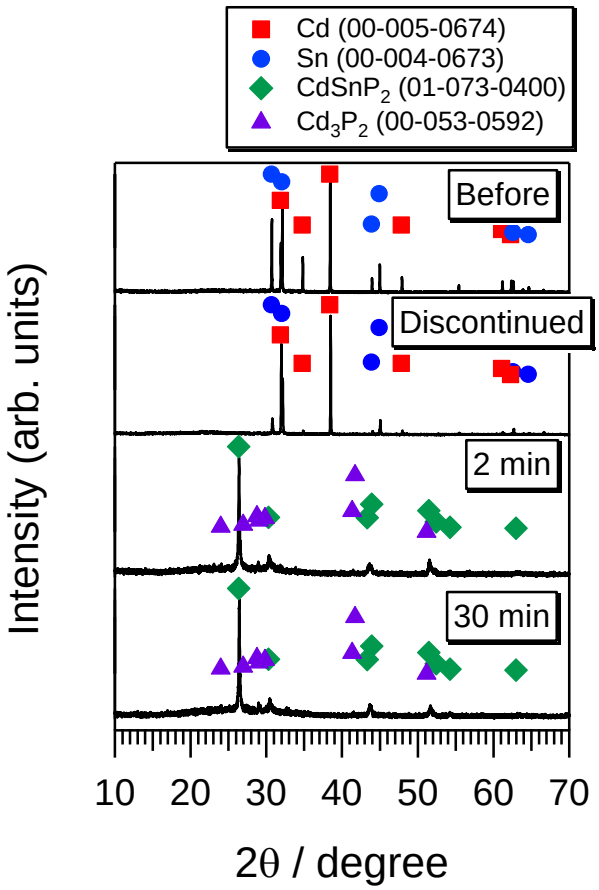

Fig. 4. XRD profiles of Cd-Sn thin films before and after phosphidation at 300 °C.

"Discontinued" indicates the sample discontinued on the way heating up to 300 °C.

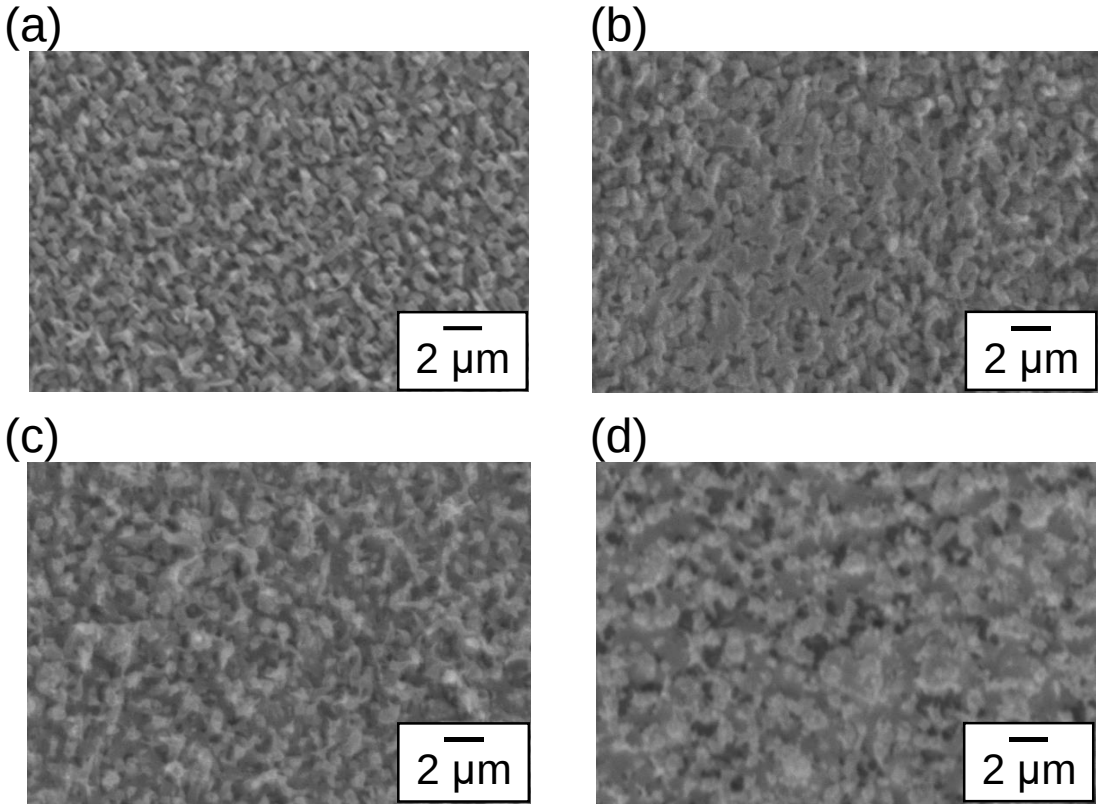

Fig. 5. SEM images of thin films (a) before phosphidation, (b) discontinued during heating up, and after phosphidation at 300 °C (c) 5 min and (d) 30 min.

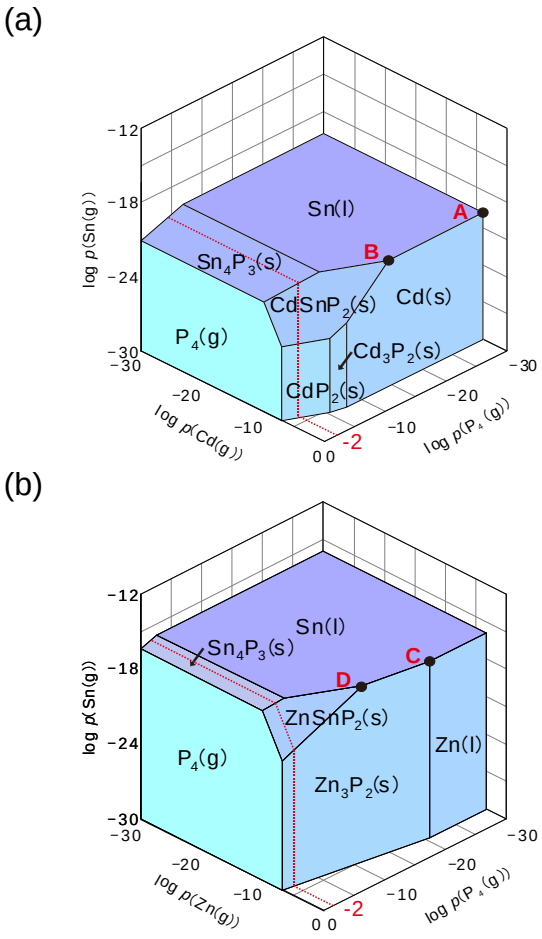

Fig. 6. Chemical potential diagrams of (a) Cd-Sn-P system at 300 °C and (b) Zn-Sn-P system at 450 °C.

■ Table of Contents (TOC) Image